

Review

Advances in Electrical Discharge Machining of Insulating Ceramics

Sergey N. Grigoriev , Marina A. Volosova and Anna A. Okunkova * 

Department of High-Efficiency Processing Technologies, Moscow State University of Technology STANKIN, Vadkovskiy per. 3A, 127994 Moscow, Russia; s.grigoriev@stankin.ru (S.N.G.); m.volosova@stankin.ru (M.A.V.)
* Correspondence: a.okunkova@stankin.ru; Tel.: +7-499-972-94-29

Abstract: There are two main ways of carrying out the electrical discharge machining of the insulating ceramics: changing the electrical and chemical properties of ceramics due to additives in producing composites/nanocomposites and changing the electrical and chemical properties in the interelectrode gap. This review summarizes and analyzes the current data on the machinability in water suspension and hydrocarbons depending on the electrical properties of the ceramic composites and assisting means such as coating and powder. There are provided the existing approaches and original methods for solving the global problem of the electrical discharge machining of insulating ceramics, suggesting further development of the existing methods since, up to now, the experimental research is non-systemic. The dependencies of the machinability on the electrical properties of conductive ceramic composites, the specific electrical resistance of the assisting coating, and the assisting powder's band gap and concentration for machining insulating ceramics are revealed. The higher the electrical conductivity, the higher the machinability of ceramic composites, and the lower the band gap, the higher the machinability for insulating ceramics. Two technological gaps were revealed in the powder's concentration that can be a particular case of logarithmic decrement of attenuation. The proposed approach suggests using assisting powder with the lower band gap.

Keywords: Al_2O_3 ; AlN; assisting means; electrical conductivity; electrical resistance; material removal rate; powder concentration; Si_3N_4 ; ZrO_2



Citation: Grigoriev, S.N.;

Volosova, M.A.; Okunkova, A.A.

Advances in Electrical Discharge Machining of Insulating Ceramics.

Materials **2023**, *16*, 5959. <https://doi.org/10.3390/ma16175959>

Academic Editor: Tassilo Moritz

Received: 28 July 2023

Revised: 22 August 2023

Accepted: 25 August 2023

Published: 30 August 2023



Copyright: © 2023 by the authors. Licensee MDPI, Basel, Switzerland. This article is an open access article distributed under the terms and conditions of the Creative Commons Attribution (CC BY) license (<https://creativecommons.org/licenses/by/4.0/>).

1. Introduction

Electrical discharge machining (EDM) can be successfully applied to single-phase ceramics, cermets, and ceramic/matrix composites as long as they exhibit electrical resistivity lower than 100–300 $\Omega\cdot\text{cm}$ [1,2]. Non-conductive ceramics such as

- most of the oxide ceramics (alumina Al_2O_3 , aluminum nitride AlN, magnesium oxide MgO , zirconia ZrO_2);
- some nitride ceramics (silicon nitride Si_3N_4 , boron nitride BN);
- oxide-nitride ceramics such as SiAlON, a solid solution of silicon nitride (Si_3N_4), where Si–N bonds are partly replaced with Al–N and Al–O bonds do not meet the minimum requirement of an electrical conductivity of 10^{-2} $\Omega\cdot\text{cm}$ to be subjected to electrical erosion [3–9] (Figure 1). However, due to their exceptional exploitation properties, they are of tremendous industrial interest for some critical applications. Secondary electrically conductive phases are incorporated to influence such insulating ceramics' electrical conductivity [10,11]. Metal-like carbides, carbonitrides, and nitrides of some transition metals that form predominantly metallic bonds (TiC, Ti(CN), TiN) serve the conductive phases in electro-conductive ceramic composites and nanocomposites based on oxide, nitride, or oxide–nitride insulating ceramics [12,13]. Metal-like carbides exhibit electrical conductivity similar to metals. They are delocalized metal bond *d*-element carbides based on iron, tungsten, tantalum, titanium, vanadium, niobium, chrome, molybdenum, and nickel, of IV–X element groups, excluding platinum-group

metals with a low electronegativity of 1.36–2.3 of Pauling’s scale and, consequently, high metallic properties [14]. These measures improve their conductive properties, enabling them to be subjected to electrical discharge machining and wear-resistance properties to operate in friction pairs (for example, for cutting tools).

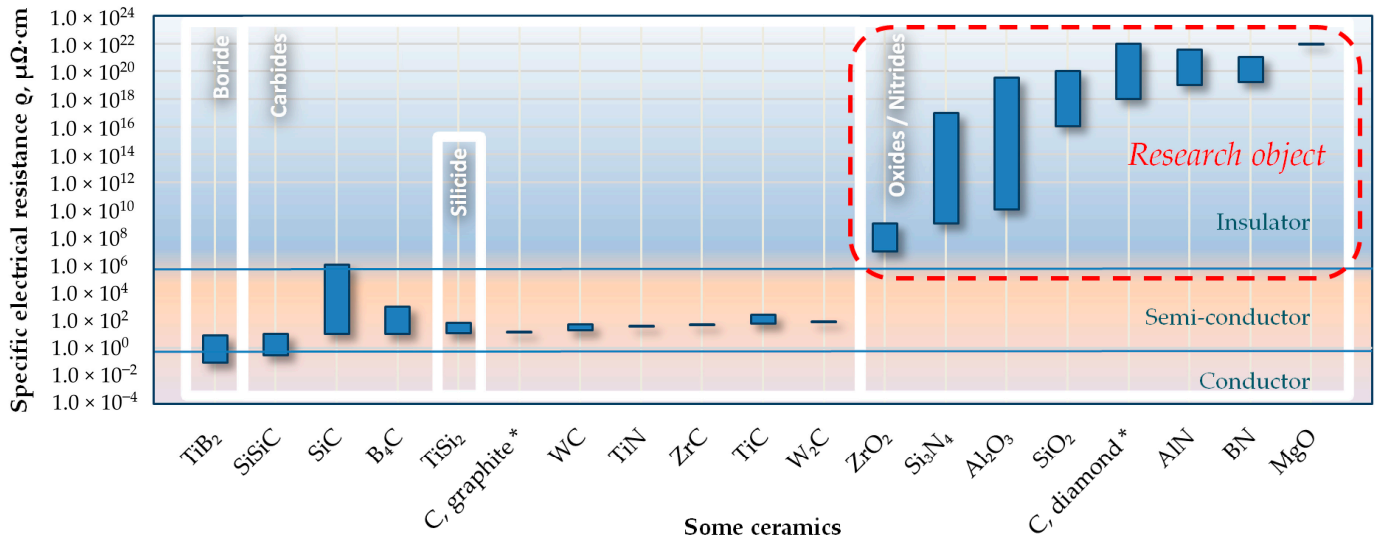


Figure 1. Specific electrical resistance ρ of some ceramics (* provided for reference).

The existing techniques of electrical discharge machining insulating ceramics suggest two main methods (Figure 2):

- By changing the properties of ceramics due to additives selected following the electrical and chemical properties of components [15,16];
- By changing the electrical and chemical properties in the interelectrode gap [17,18].

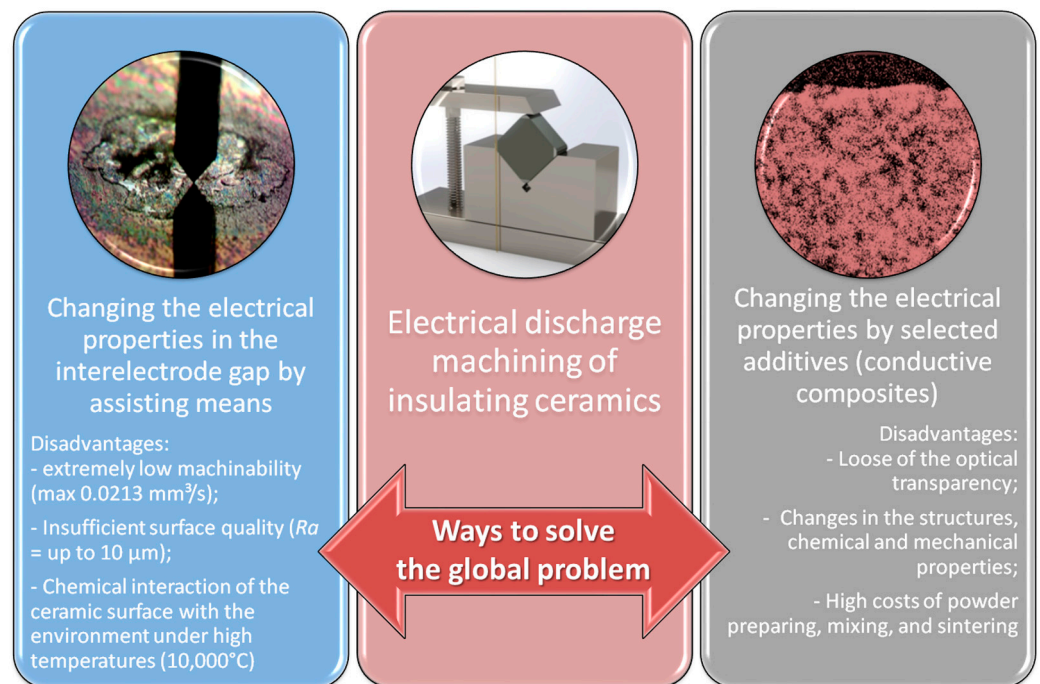


Figure 2. Two main ways to solve the global problem of electrical discharge machining of insulating ceramics and their disadvantages.

The main disadvantage of the first method is the complete and expensive nanomodification of the material with the loss of such properties as optical transparency. The disadvantage of the second method is its low efficiency concerning insulating ceramics, associated with the above-described features. This work aims:

- To review the recent advances and developments in the electrical discharge machining of insulating ceramics;
- To summarize and analyze the current data on the machinability of conductive ceramic composites and the insulating ceramics based on oxides and nitrides in water suspension and hydrocarbons depending on the electrical properties of the ceramics and assisting means;
- To search the approaches and original methods for solving the global problem of the electrical discharge machining of insulating ceramics.

The proposed approach can be extended to develop solutions for electrical discharge machining other insulating materials (including ones filled with glass fiber).

2. Electrical Conductivity of Insulating Ceramics and Conductive Composites

Typical ceramics are chemical compounds based on polar bonding. The absence of slip planes makes them extremely brittle by comparison with, for example, steel. When ceramic pieces have been manufactured, they cannot be subjected to heat treatment to induce deliberate changes in their structure. Whereas steels possess a dense structure following crystallization and recrystallization, ceramics fundamentally constitute a multiphase system comprising crystals, a binder phase, and pores [19].

Natural electrical conduction by free lattice electrons makes some carbide, carbonitride, and nitride ceramics electrically conductive (delocalized metal bond *d*-element carbides of IV–X groups excluding platinum group metals). For insulating ceramics (mainly oxide ceramics and nitride ceramics of some elements of III–V groups such as AlN), two mechanisms are utilized to make engineering ceramics electrically conductive:

- Doping with conductive elements;
- Incorporating impurity atoms [20].

Electrically conductive carbides, carbonitrides, and nitrides serve as usual doping components to make insulating ceramics electrically conductive. These ceramics are primarily used as doping components because they are chemically neutral to oxygen. It should be noted that other nitrides mainly exhibit unstable chemically active and explosive properties (Cu_3N , Mg_3N_2 , Pb_3N_2 , Zn_3N_2) and decomposes to oxides.

The electrical conductivity of oxide or nitride ceramic composites can be improved by combining the transition-metal carbide or nitride particles with the electrical conductivity of $\rho = 10^2\text{--}10^6 \mu\Omega\cdot\text{cm}$ and the high strength and wear resistance of the matrix [21]. The improved high-performance ceramic matrix presents a fine-grained microstructure (Table 1) that does not deteriorate to operating temperatures close to 1000 °C. The Vickers hardness and fracture toughness of the composites increased with TiC phase addition into Al_2O_3 -TiC composites containing 30 and 40 vol.% TiC. The composite with 40 vol.% TiC showed the highest flexural strength ($687 \pm 39 \text{ MPa}$), fracture toughness ($7.8 \pm 0.4 \text{ MPa}\cdot\text{m}^{1/2}$), and hardness ($22.3 \pm 0.3 \text{ GPa}$) with a homogeneous distribution of the second phase within the ceramic matrix [22]. The conductive properties mainly depend on conductive additives concentration [23] when the mechanical properties do not correlate with the content of the ceramic basis (Al_2O_3 -content, Table 1).

Table 1. Electrophysical and mechanical properties of Al₂O₃-based ceramics.

Type of Ceramics	Specific Electrical Resistance ρ at +20 °C, $\Omega \cdot \text{mm}^2/\text{m}$	Flexural Strength, MPa	Fracture Toughness, $\text{MPa} \cdot \text{m}^{1/2}$	Vickers Hardness, GPa	Average Particle Size, μm	Reference
Al ₂ O ₃ (99.8 wt.%)	10^{12} – 10^{14}	630	4.3	20.00	Not provided	[23,24]
Al ₂ O ₃ (99 wt.%)	Not provided	500	3.5	18.65	3.0–4.0	[25]
Al ₂ O ₃ (85 vol.%)–SiC (15 vol.%)	Not provided	850	6.5	22.00	1.0–2.0	[25]
Al ₂ O ₃ (70 vol.%)–TiC–TiN (22.5 vol.% of TiC + 7.5 vol.% of TiN)	Not provided	890	5.6	21.80	0.14–1.0	[23]
Al ₂ O ₃ (70 vol.%)–TiC (30 vol.%)	3.382	643 ± 48	7.1 ± 0.3	22.80 ± 0.30	0.53–0.6	[26]
Al ₂ O ₃ (70 vol.%)–TiN (30 vol., Cortinitis)	Not provided	640	4.5	18.65–20.00	2.0	[25,27]
Al ₂ O ₃ (60 vol.%)–TiC–TiN (10 vol.% of TiC _{μm} + 10 vol. of TiC _{nm} + 20 vol.% of TiN)	Not provided	881.4	7.8	20.80	0.14–1.0	[23]
Al ₂ O ₃ (60 vol.%)–TiC (29.85 vol.% of TiC + 0.5 vol.% of MgO)	Not provided	630	5.2	17.80	1.39	[28]
Al ₂ O ₃ (60 vol.%)–TiC (40 vol.%)	Not provided	600	4.2	20.00	2.0–3.0	[25]
Al ₂ O ₃ (60 vol.%)–TiC (40 vol.%)	0.589	687 ± 39	7.8 ± 0.4	23.30 ± 0.30	0.53–0.6	[26]
Al ₂ O ₃ (60 vol.%)–TiC (40 vol., commercial sample)	3.510	637	3–5	13.50–14.00	Not provided	[26]
Al ₂ O ₃ (40 vol.%)–TiC (55 vol.% of TiC + 2.25 vol.% of Mo + 2.25 vol.% of Ni)	Not provided	890	7.8	Not provided	0.5	[22]
Al ₂ O ₃ (35 vol.%)–TiC (55 vol.% of TiC _{μm} + 5 vol.% of TiC _{nm} + 2.25 vol.% of Mo + 2.25 vol.% of Ni)	Not provided	840	7.5	Not provided	0.04	[22]

The conductors have specific electrical resistance $\rho < 10^{-5} \Omega \cdot \text{m}$ as the specific electrical resistance of dielectrics is $\rho > 10^8 \Omega \cdot \text{m}$. The value of specific electrical resistance for produced conductive ceramic with 30 vol.% of TiC is close to the value for carbon in the form of graphite ($\rho = 8 \times 10^{-6} \Omega \cdot \text{m}$) [28]. Thus, the samples of sintered Al₂O₃ + TiC ceramic with more than 30 vol.% of TiC are suitable for electrical discharge machining [25–27]. The electrical conductivity of some conductors can fluctuate in the range of 10 – 10^{-12} S/m ($\rho = 10^{-1}$ – $10^{12} \Omega \cdot \text{m}$) and also depends on many factors, including temperature and crystal lattice orientation (some materials, such as carbon, exhibit anisotropy of electrical properties) [29–31].

The addition of carbon nanotubes (CNTs) to the zirconia matrix in zirconia-based composites induces a substantial increase in electrical conductivity associated primarily with the fact that zirconium and zirconium carbide formed because of the thermochemical reaction have similar electrical conductivity (Table 2) [24,32–35]. The formation of zirconium carbide occurs through the thermal dissociation of zirconium dioxide and the reduction of lower oxides with carbon:



where T_1 and T_2 are the subjects of a separate study.

Table 2. Electrical properties of some Zr-containing materials.

Material	Electrical Conductivity σ , S·m ⁻¹	Specific Electrical Resistance ρ at +20 °C, $\Omega\cdot\text{m}$	Specific Electrical Resistance ρ^* at +20 °C, $\Omega\cdot\text{mm}^2/\text{m}$	Thermal Conductivity α at +20 °C, W·m ⁻¹ ·K ⁻¹	Reference
ZrO ₂ † (Insulator)	10 ⁻⁶ –10 ⁻¹²	10 ⁶ –10 ¹²	10 ⁸ –10 ¹⁴	1.7–2.7	[32–34]
ZrO ₂ + 0.5 wt.% CNT ‡ (Insulator)	1.0 × 10 ¹	1.0 × 10 ⁻¹	1.0 × 10 ¹	3.3 §	[35]
ZrO ₂ + 1 wt.% CNT (Insulator)	3.16 × 10 ²	3.16 × 10 ⁻³	3.16 × 10 ⁻¹	2.8 §	[35]
ZrO ₂ + 2 wt.% CNT (Insulator)	7.50 × 10 ²	1.33 × 10 ⁻³	1.33 × 10 ⁻¹	Not provided	[35]
ZrO ₂ + 3 wt.% CNT (Insulator)	8.66 × 10 ²	1.15 × 10 ⁻³	1.15 × 10 ⁻¹	Not provided	[35]
ZrO ₂ + 4 wt.% CNT (Insulator)	1.0 × 10 ³	1.0 × 10 ⁻³	1.0 × 10 ⁻¹	2.6 §	[35]
ZrC † (Conductor)	2.0 × 10 ⁶	5.0 × 10 ⁻⁷	5.0 × 10 ⁻⁵	11.6	[36,37]
Zr † (Conductor)	2.27 × 10 ⁶	4.41 × 10 ⁻⁷	4.41 × 10 ⁻⁵	22.7	[38]

* calculated for convenience; † given for references; ‡ CNT is carbon nanotubes; § obtained by spark plasma sintering at 1350 °C.

Simultaneously, it provokes relatively slight thermal conductivity changes (Table 2). The specific electrical conductivity of amorphous oxide ceramics and semiconductors increases significantly with an increase in temperatures since the concentration and mobility of charge carriers are exponentially dependent on temperature (t , °C) as was approximated:

$$\sigma = \sigma_0 \cdot e^{\beta \cdot t}, \quad (4)$$

where σ_0 is the value of specific electrical conductivity at normal temperature, and β is the temperature coefficient (1/°C). It can be presented as follows (Figure 3). As can be seen with $\rho > 10^8 \Omega\cdot\text{m}$ and variable value β (for different materials), it is possible to achieve superconductivity conditions at the lowest and highest temperatures. The graphs for other types of dielectric and semiconductive oxide and nitride ceramics have similar trends and vary in σ_0 . For crystalline ceramics, the observed increase in specific and volumetric electrical conductivity is less pronounced, and for metals, it has the opposite tendency [24,39].

An introduction of 30–40 vol. % TiN_x (x is in the range of 0.6–1.2; electrical resistivity ρ at +20 °C of 1.0×10^{-7} – $4.0 \times 10^{-7} \Omega\cdot\text{m}$ in bulk; 3.0×10^{-7} – $1.0 \times 10^{-6} \Omega\cdot\text{m}$ by plasma vapor deposition (PVD); 2.0×10^{-6} – $1.0 \times 10^{-4} \Omega\cdot\text{m}$ by chemical vapor deposition (CVD)) into Si₃N₄ (1.0×10^4 – $1.0 \times 10^{13} \Omega\cdot\text{m}$) provides an electrically conductive composite with a decreased electrical resistivity of $\sim 10^{-5} \Omega\cdot\text{m}$. Introducing the conductive component also improves mechanical properties such as fracture toughness, strength, and wear resistance [40–42].

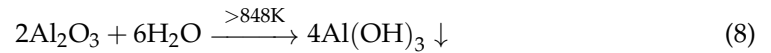
The problem with Al-based ceramics is in forming pyrophoric ionic salt-like carbides Al₃C₄ or Al₂(C₂)₃ (yellow crystals), where Al₃C₄ is methanide with (C = C)⁴⁻ and Al₂(C₂)₃ is acetylenide with (C = C)²⁻ that exhibit insulating properties as for Be₂C, Li₄C, Mg₂C (C⁴⁻) or Ag₂C₂, CuC₂, CaC₂, Li₂C₂, BaC₂ (C₂²⁻) unlike metal-like carbides (Cr_xC_y, Fe_xC_y, Mo_xC_y, Nb_xC_y, Ni_xC_y, Ta_xC_y, TiC, V_xC_y, WC). At a temperature of the thermal decomposition (dissociation), Al₂O₃ ceramics dissociate as follows [24,43]:



or



Electrical erosion of alumina in the absence of hydrocarbons can be accompanied by a chemical reaction of dissociated molecules that compose the following insoluble sediment, which decomposes when heated above 848 K:



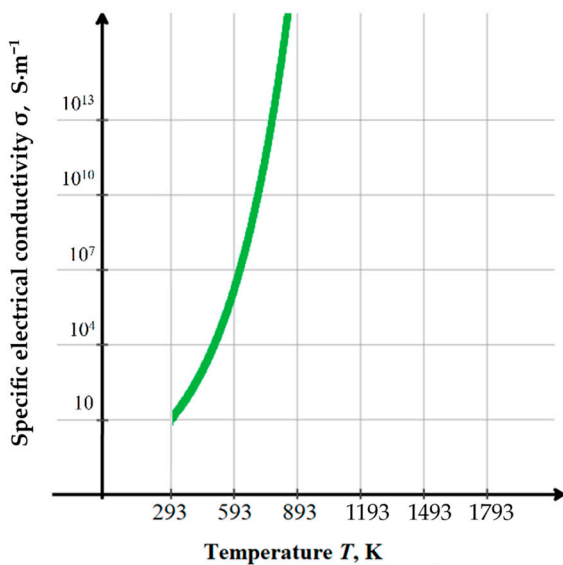
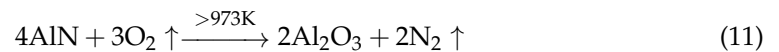
A similar issue is related to the dissociation of AlN:



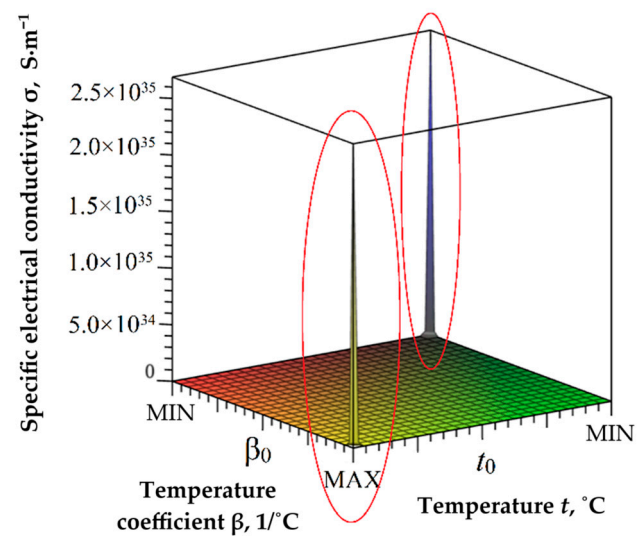
The released aluminum reacts with the carbon similarly to (5). It can hydrolyze slowly in water:



At the atmosphere, nanofilms of alumina with a thickness of several nanometers are formed at temperatures above 973 K, which can keep from hydrolysis to temperatures above 1643 K. Above this temperature, bulk oxidation occurs:



(a)



(b)

Figure 3. Theoretical specific electrical conductivity σ for dielectric and semiconductive oxide and nitride ceramics (by the example of ZrO_2): (a) with $\beta = \text{const}$, where $t_0 = +20\text{ }^\circ\text{C}$ and $\sigma_0 = 10\text{ S}\cdot\text{m}^{-1}$; (b) with the theoretically varied the temperature coefficient β , where $t_0 = +20\text{ }^\circ\text{C}$ and $\sigma_0 = 10^{-8}\text{ S}\cdot\text{m}^{-1}$, extremes (marked red) may correspond to superconducting conditions.

3. Advances in Electrical Discharge Machining of Ceramics

3.1. Electrical Discharge Machining of Conductive Ceramic Composites

The machinability of conductive ceramic composites in electrical discharge machining is presented in Table 3. A graphical presentation of the data compared with the maximal achievable machinability for the conductive materials (aluminum alloys, pure chrome, and copper) is shown in Figure 4.

Table 3. Machinability of conductive ceramic composites in electrical discharge machining.

Material	Workpiece Thickness/Machined Depth, mm	Electrical Conductivity σ , $S \cdot m^{-1}$	Technology of Producing	Electrode Tool	Main EDM Factors	Dielectric Medium	Machinability	Reference
Al ₂ O ₃ -TiC (30 wt.%)	10	2.60×10^5 (3.77 $\Omega \cdot mm^2/m$)	WEDM	Brass wire, $\varnothing 250 \mu m$	$V_0 = 108 V$; $f = 5 kHz$; $D = 1 \mu s$	Deionized water, no flushing	0.4 mm/min (feed rate, no obstacles)	[11]
Al ₂ O ₃ -TiC (30 wt.%)	2–4	2.96×10^5	WEDM	Brass wire, $\varnothing 250 \mu m$	$V_0 = 270 V$; $I_e = 0.05 A$	Deionized water with conductivity of 0.1 $\mu S/cm$, no flushing	Suitable for EDM	[26]
Al ₂ O ₃ -TiC (40 wt.%)		1.70×10^6					Suitable for EDM	[26]
SiAlON-TiN (10 wt.%)	3	$9.80 \times 10^{-3} *$ ($1.02 \times 10^2 \Omega \cdot m$)	WEDM	Brass wire, $\varnothing 250 \mu m$	$V_0 = 72 V$; $I_e = 1.9 A$; $D = 2 \mu s$ (relaxation)	Deionized water with conductivity of 0.1 $\mu S/cm$, no flushing	Suitable for EDM	[44]
SiAlON-TiN (20 wt.%)		$6.25 \times 10^3 *$ ($1.6 \times 10^{-4} \Omega \cdot m$)					Suitable for EDM	[44]
Si ₃ N ₄ -TiN (~30 wt.%)	0.605 ($\times \varnothing 0.123 mm$, programmed depth of 0.5)	Did not exhibit any (coated with Ag varnish of 20 μm), calculated circuit linear resistance of $4.78 \times 10^5 \Omega/m$	Micro-EDM (ED drilling)	WC rod (6% cobalt binder) of $\varnothing 115 \mu m$	$V_0 = 165, 180 V$; $I_e = 70 A$; $D = 6 \mu s$	Hydrocarbon oil (HEDMA-111)	0.010–0.011 mm/min for 58 min of machining or $7.76 \times 10^{-6} mm^3/s$ † for an area of 0.045 mm ²	[45]
ZTA-TiC (alumina + 17 vol.% of zirconia, 1.5 vol.% of yttria, 24 vol.% of TiC)	10	4.93×10^3	ED drilling	Copper tube electrode (Typ-D) of $\varnothing 2000 \mu m$	$V_0 = 130 V$; $I_e = 15, 20 A$; $D = 40, 60 \mu s$	Oil-based fluid with flushing 1–6 L/h	Theoretical feed rate of ~0.8–1.0 mm/min (active feed rate/proportion of effective pulses)	[46]
ZrB ₂ -SiC (20 wt.%, short fibers)	0.2 ($\times \varnothing 1.0 mm$)	Not provided	Micro-EDM (ED drilling)	WC rod electrode of $\varnothing 300 \mu m$	$V_0 = 70 V$; $I_e = 29 A$; $D = 0.7 \mu s$	Hydrocarbon oil	$6.14 \times 10^{-8} mm^3$ per discharge (18.26 mm/min for an area of 0.28 mm ²) ‡	[47]
ZrB ₂ -SiC (20 wt.%, whiskers)		Not provided				$V_0 = 71 V$; $I_e = 29 A$; $D = 0.7 \mu s$		$6.38 \times 10^{-8} mm^3$ per discharge (18.97 mm/min for an area of 0.28 mm ²) ‡

V_0 is the operational voltage; f is the frequency; D is the pulse duration; I_e is the operational current; * experimentally obtained; † calculated for convenience; ‡ it should be noted that the conventional material removal rate for wire electrical discharge machining (WEDM) of conductive materials is 0.2–12 mm/min [48], but practice dictates that in most of the cases it is 0.8–1.0 mm/min, and maximum for aluminum is about 4–6 mm/min [49], and it is highly possible that authors have been mistaken in their calculations or did not take into account electrode relaxation time in discharge timing and the actual linear material removal rate should not exceed 1.82 and 1.90 mm/min, correspondingly.

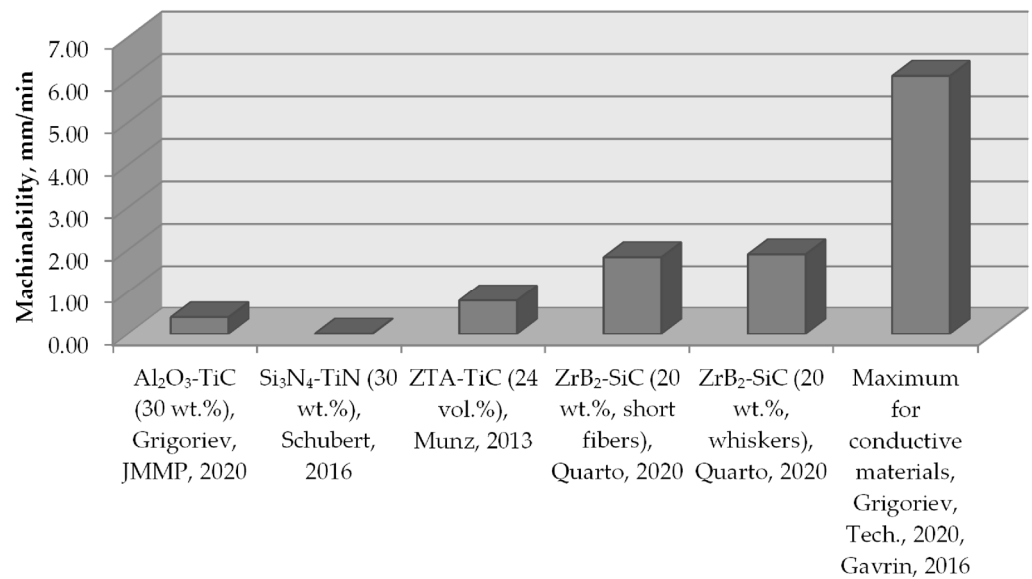


Figure 4. The graphical presentation of conductive ceramic composites’ machinability via electrical discharge machining comparing with the maximal achievable machinability for the conductive materials, where Grigoriev, JMMP, 2020 [11], Schubert, 2016 [45], Munz, 2013 [46], Quarto, 2020 [47], Grigoriev, Tech., 2020 [48], Gavrin, 2016 [49].

In [26], it was shown that at 30 vol.% of TiC in Al₂O₃-TiC composite, the electrical conductivity corresponds to the adequate level that exceeds the percolation threshold, while Al₂O₃-TiC composite exhibits conductivity close to the conductivity of pure titanium at 40 vol.% of TiC. These types of ceramic composites have been known since the mid-1970s [29–31]. Still, many research groups conduct experiments on improving their properties by experimenting with technological factors and the dispersion of precursors.

The authors of [44] propose electrically conductive homogenous and dense SiAlON-TiN (10 wt.% and 20 wt.%) ceramic nanocomposite produced by advanced spark plasma

sintering at 1700 °C suitable for wire electrical discharge machining. The nanocomposite with 20 wt.% TiN showed specific electrical resistance ρ lower than 1–3 $\Omega\cdot\text{m}$.

A. Schubert et al. experimentally investigated electrical discharge milling (ED milling) parameters of titanium nitride toughened silicon nitride ($\text{Si}_3\text{N}_4\text{-TiN}$) [45]. As $\text{Si}_3\text{N}_4\text{-TiN}$ is decomposed at a high temperature in the discharge gap, it exhibits a particular ablation behavior that allows machining with a material removal rate of 200% compared to insulating ceramics of $\text{Al}_2\text{O}_3\text{-ZrO}_2$ type. The maximum bore depth was 605 μm . The material removal rate was increased by increasing the power (Figure 5). A volume fraction of 30% of the conductive TiN phase is above the percolation threshold, and the electrical conductivity is provided by the TiN network [50]. For hot-pressed $\text{Si}_3\text{N}_4\text{-TiN}$ (30vol.%), lowering the sintering temperature from 1700 to 1500 °C decreases resistivity from 0.18 to 0.004 $\Omega\cdot\text{cm}$. The percolation threshold (V_c) is determined as follows:

$$V_c = 100 \cdot \left[\frac{1}{1 + \left(\frac{4}{\theta} \cdot \frac{D_i}{d_c} \right)} \right], \quad (12)$$

where θ is a quantity of the conductive particles on the surface of the insulating ones; D_i and d_c are the diameters of the insulating and conductive particles. A higher diameter ratio (D_i/d_c) results in a lower V_c . The decomposition of the conductive ceramic composites unavoidably leads to a porous and foamy microstructure shown in [11] and correlates with analytic results of plasma chemistry [51]. During machining in oil, $\text{Si}_3\text{N}_4\text{-TiN}$ decomposes on conductive carbides (TiC, SiC), and alumina–zirconia forms conductive ZrC [47] and non-conductive pyrotechnically active Al_3C_4 [52,53]. The formed Al_3C_4 can actively hamper processing by changing the discharge gap's electrical conditions since hydrocarbon oil exhibits better electrical conductivity (1.9–4.3 $\Omega\cdot\text{m}$ depending on oil purity) than insulating ceramics ($\leq 10^{-4}$ $\Omega\cdot\text{m}$) [11].

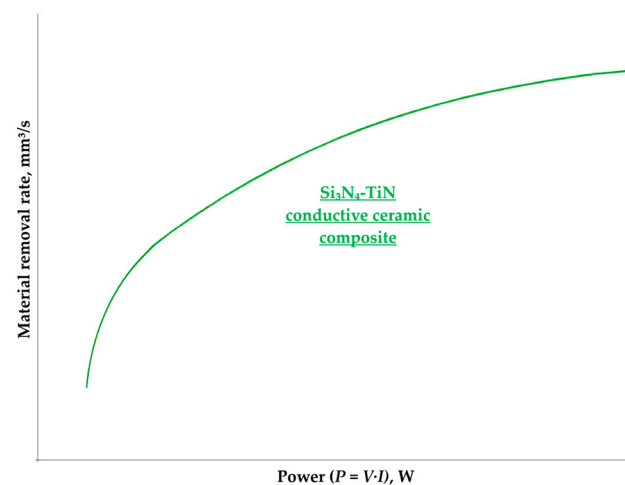


Figure 5. The dependence of the machinability on power for $\text{Si}_3\text{N}_4\text{-TiN}$ conductive ceramics in electrical discharge milling (logarithmic regression), based on [45].

M. Munz et al. [46] added TiC to zirconia and investigated the electrical discharge drilling of ZTA-TiC ceramics. They studied material removal rate, discharge energy, pulse shapes, peak current, and discharge time. They observed that the triangle pulse with a current of 20 A or less is better than the rectangle pulse for the electrical discharge drilling.

The suitable factors to accomplish the electrical discharge machining of conductive ceramic composites are the following:

- Assisting electrode is not required;
- Operational current of 0.05 A [26], 20 A or less [45];
- Operational voltage varies from 20 and 120 to 270 V [26];

- Frequency is 5 kHz;
- Discharge gap depends on the electrical conductivity of the workpiece material and is 10–200 μm .

3.2. Electrical Discharge Machining of Insulating Ceramics

D. Hanaoka et al. mentioned that the electrical conductivity limit was below $4 \times 10^{-2} \text{ S}\cdot\text{m}^{-1}$ [54]. The machining speed increases as the peak current and pulse width increase. The removal mechanism changes as the pulse width increases. As analyzed from the experiments, when the pulse width was set as 20–30 μs , the machining was stable, and a smoother machined surface was obtained. The pulse interval is not the dominant factor in increasing the machining speed but in improving the machined surface accuracy [55]. The material removal rate of Al_2O_3 and ZrO_2 using adherent copper foil rose with an increase in peak current and pulse duration (Figure 6a). Additionally, the electrode wear rate of Al_2O_3 and ZrO_2 increased with peak current but reduced with pulse duration [56]. However, when the pulse duration exceeded 200 μs , the tool wear rate during the Al_2O_3 ceramic machining demonstrated the reverse trend: the tool wear rate slightly increased at a pulse duration longer than 200 μs . The surface roughness of Al_2O_3 and ZrO_2 increased with peak current and pulse duration (Figure 6b). Moreover, the surface roughness of the Al_2O_3 ceramic after electrical discharge machining was higher than for the ZrO_2 ceramic at identical machining conditions that correlated with the plasma chemical nature of the processes between electrodes in the presence of heat higher than 3500 $^\circ\text{C}$, which remained unexplained in the paper. The surface integrities of ZrO_2 revealed more machining debris adhered to the machined surface, and the Al_2O_3 machined surface and thermal spalling features were rougher than for ZrO_2 . In general, the machining performance (material removal and tool wear rates) of ZrO_2 with the copper adherent tape is better than Al_2O_3 with the same adherent. H. Zhang et al. [57] developed a technique to provide pulse generators with self-adapting voltage-adjusting for the electrical discharge machining of Al_2O_3 insulating ceramic. They demonstrated that the pulse generator could improve energy availability and discharge flexibility.

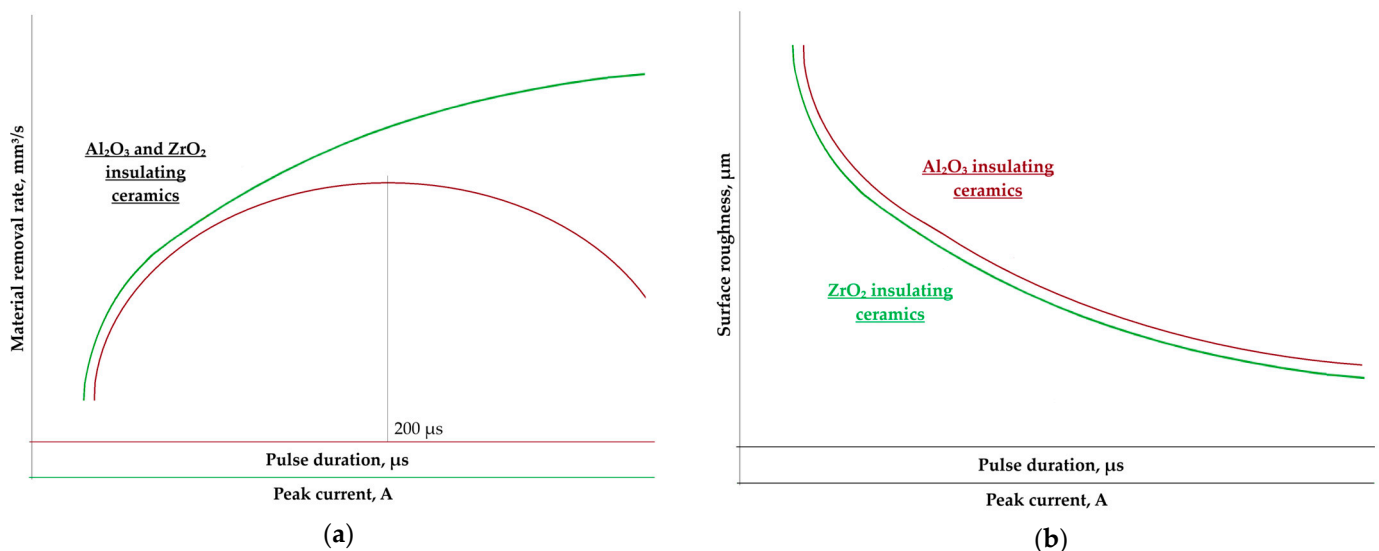


Figure 6. The dependence of the machinability on peak current (logarithmic regression) and pulse duration (quadratic regression or exponential attenuation) (a); the dependence of the surface roughness on peak current and pulse duration (logarithmic regression) (b) for Al_2O_3 and ZrO_2 insulating ceramics in electrical discharge machining, based on [56].

N. Ojha et al. [58] monitored the electrical signals when machining copper and non-conductive ceramic Si_3N_4 . Voltage and current sparks' signals were shown. They demonstrated that the most remarkable differences were a significant decrease for Si_3N_4 in the

ringing behavior of the voltage signal and the absence of reverse current for Si_3N_4 , and a decrease in the peak current value detected in the case of Si_3N_4 . H. Gotoh et al. [59] used a unique technique for machining insulating ceramics Si_3N_4 with electrical discharge milling. They used a method in which the pulse discharge was longer than the pulse duration. Hence, the electrically conductive layer is created on the insulating ceramic surface, enabling machining.

The results of applying the assisting electrode technique primarily depend on the method of pre-coating the insulating ceramic workpiece and the main properties of the film (adhesion, thickness, chemical composition) (Table 4). The graphical presentation of the machinability of Al_2O_3 insulating ceramics is shown in Figure 7. As seen, the machinability in oil is 2.54 times higher than in water. From all the used assisting means, copper tape in combination with TiO_2 powder provides higher machinability in the water-based dielectric medium. After processing, the film can be chemically removed from the ceramic surface with acetone, $\text{K}_2\text{CrO}_4\text{-H}_2\text{SO}_4$ mixture, or other solvents [60,61].

Table 4. Types of assisting electrodes for electrical discharge machining of aluminum-containing insulating ceramics.

Assisting Electrode Material	Assisting Electrode Shape/Thickness, μm	Type of Deposition	Primary Electrode Material and Shape	Technology	Dielectric Medium	Insulating Workpiece Material	Maximum Depth, μm	Machining Time, min	Material Removal Rate, mm^3/s	Reference
Copper	Foil/Not provided	Adhesive	Not provided	EDM	Kerosene	Al_2O_3 , ZrO_2	Not provided	Not provided	Not provided	[56]
	Sheet/Not provided	Not provided	Steel	ED Milling	Water-based emulsion	Al_2O_3	Not provided	Not provided	Not provided	[62]
	Foil/60 μm	Adhesive	Cu, 5000 \times 5000 μm	EDM	Kerosene	Al_2O_3 (92% of purity)	1500	$\sim 120^*$ (37.5 $\text{mm}^3/0.0051$ $\text{mm}^3/\text{s} = 7352$ s)	0.0051	[63]
	Triple layered copper tape/150 μm	Adhesive	Cu-W, $\varnothing 600$ μm	Micro-EDM	Hydrocarbon (mineral) oil, no flushing, no rotation Deionized water + TiO_2 particles of $\varnothing 10$ μm (150 g/L)	AlN	700 (from tape surface) 52 \times 111 \times 7250 (D \times W \times L)	120	0.0001* (0.79 $\text{mm}^3/7200$ s)	[64]
	Copper tape/40 μm	Adhesive	Brass wire, $\varnothing 250$ μm	WEDM	Hydrocarbon (mineral) oil HEDMA-111	Al_2O_3	731 \times $\varnothing 120$ (for programmed depth of 500 μm)	0.17 (10 s)	0.0084	[65]
Silver	Varnish (45% of Ag) applied with a Paintbrush/20 μm	Adhesive	A WC rod with 6% of Co binder, $\varnothing 115$ or 500 μm †	Micro-EDM (proposed for ED Milling)	Hydrocarbon (mineral) oil HEDMA-111	ATZ ceramic composite (10% of Al_2O_3 toughened ZrO_2)		43	Not provided	[45]
	Double paint layer of Ag coating with Ag nanopowder in between/Not provided	Diffusion, baked sandwich at 900 $^\circ\text{C}$ for 60 min	Cu-W, $\varnothing 600$ μm	Micro-EDM	Hydrocarbon (mineral) oil, no flushing, no rotation	AlN	700 (from coating surface)	600	0.00002* (0.79 $\text{mm}^3/36,000$ s)	[64]
Carbon	Polymer-based material containing carbon powder/Not provided	Adhesive, heated at 150 $^\circ\text{C}$	Cu pipe of $\varnothing 3500$ μm with a hole of $\varnothing 3000$ μm	EDM	Kerosene with graphite powder of $\varnothing 30$ μm (7–10 g/L), flushing at 1.5 bar pressure	Al_2O_3	~ 5000	~ 235	0.0213	[66]
Ag + Cu	Ag nanoparticles sandwiched between two paint layers of Ag coating with Cu tape on top/Not provided	Diffusion, baked sandwich at 900 $^\circ\text{C}$ for 60 min	Cu-W, $\varnothing 308$ μm	Micro-EDM	Hydrocarbon (mineral) oil with Ag nanoparticle (0.1 g/L), no flushing, no rotation	AlN	1693 (from coating surface)	150	0.0006* (0.50 $\text{mm}^3/9000$ s)	[64]
Ni + Cr	Cu-Ag doubled-layered coating (Cu-tape + polymer glue with Ag-powder)/300 μm	Adhesive	Brass wire, $\varnothing 250$ μm	WEDM	Deionized water + ZnO particles of $\varnothing 10$ μm (14 g/L)	Al_2O_3	980 (from workpiece surface)	Not provided	0.0032–0.0053	[67]
	Ni-Cr PVD coating/12 μm	Diffusion	Brass wire, $\varnothing 250$ μm	WEDM	Deionized water + SnO particles of $\varnothing 10$ μm (150 g/L)	Al_2O_3	50 \times 320 \times 4000 (D \times W \times L)	0.5 (30 s)	0.0014	[68]

* calculated for convenience; † the authors provide two different values in two paragraphs.

There are several types of coating to accomplish the process, such as copper assisting electrode [56,62–65], silver varnish [45,64], carbon conductive layer [66], multimerial sandwich coatings [64,67], and Ni-Cr coating by plasma vapor deposition [68]. The assisting electrode made of copper tape can be removed easily from the AlN [64], Al_2O_3 [65], and ZrO_2 [69] ceramic surface after the machining. There are also examples of electrical discharge machining of Si_3N_4 ceramics in TiO_2 water-based suspension using conductive TiN coating deposited by plasma vapor deposition [70]. Any plasma vapor deposition coatings are difficult to remove after machining due to diffusion between the insulating workpiece and coating materials. However, the authors propose using assisting coating as a multifunctional one that provides conductive properties to the surface layer of the insulating workpiece and is used as a wear-resistant coating to prolongate the operational life of the Si_3N_4 ceramic cutting insert. In [66], it was experimentally shown that machin-

ability strongly depends on electrical resistivity for TiO_2 , SiC , and ZrO_2 ceramics during electrical discharge drilling when there is probably other nature (obviously, thermochemical combining with electrophysical) in Al_2O_3 and SiO_2 ceramics machining, but the trends are similar.

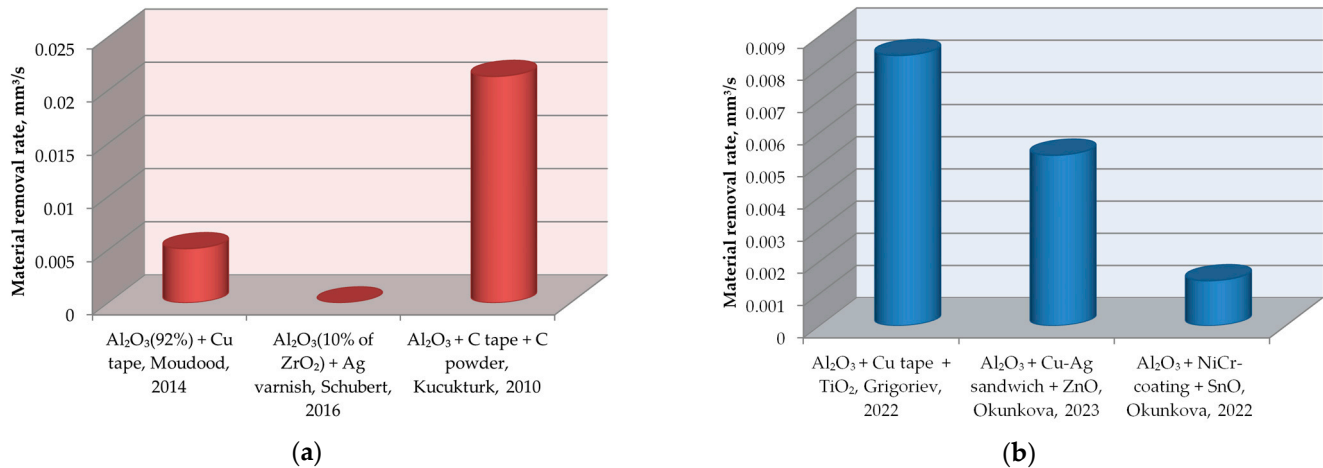


Figure 7. The graphical presentation of Al_2O_3 insulating ceramic machinability via electrical discharge machining: (a) in hydrocarbons, (b) in water suspension, where Schubert, 2016 [45], Moudood, 2014 [63], Grigoriev, 2022 [65], Kucukturk, 2010 [66], Okunkova, 2023 [67], Okunkova, 2022 [68].

The authors that research the electrical discharge machining of ZrO_2 ceramics in hydrocarbon oil [56,66,71,72] report on forming conductive ZrC with the same conductivity as pure Zr [24]. Electrical discharge machining of aluminum-containing insulating ceramics in oil presents an unsolved scientific problem related to the high electronegativity of aluminum, which is very active towards oxygen and forms non-conductive carbides in its absence that are mistakenly named pyrolytic carbon. In [66], it was reported that not only “pyrolytic carbon” was identified in the working area.

A typical crater-like surface was detected during the electrical discharge machining of ZrO_2 ceramics [45]. Thermal cracks and cleavages characterize the AlN ceramic surface [64]. The Al_2O_3 ceramic surface [68] is characterized by the traces of the thermal sublimation and drop-like deposition of the secondary structure of the compositions of secondary order formed by the products of the interaction of the decomposition of ceramics, assisting powder and dielectric medium.

The authors [64] consider chemical and plasma vapor deposition methods to be time-consuming and require costly equipment compared with the technique of AlN ceramics coating with the labor-intensive two-layered Ag sandwich coating with Ag nanoparticles between them additionally covered with copper tape. However, the PVD technique has demonstrated impressive results with a material removal rate of $0.0014 \text{ mm}^3/\text{s}$ in machining Al_2O_3 ceramics [68], which is more than two times higher than $0.006 \text{ mm}^3/\text{s}$ for AlN ceramics [64]. The actual problem of any plasma deposition technique of copper and silver coating is related to droplet formation [73,74] and coating low adhesion to insulating ceramics with a coating thickness above $3\text{--}4 \mu\text{m}$ [75,76]. At the same time, there is a global problem of discharge impulse reinitiating in the working zone when most of the coating is sublimated and decomposed in the dielectric medium. In this context, the Ni-Cr coating [68] has shown better prospects: it has smoother surface characterization when deposited on the insulating ceramic surface, exhibits better adhesion at the coating thickness up to $15 \mu\text{m}$, and it can form intermetallic compounds of Al_xNi_y type (when $x = 1, 3, \dots$ and $y = 1, 3, \dots$) [77] during coating sublimation and decomposition. These types of compounds exhibit superconductive properties and have prospects for future development. It should be noted that the addition of silver nanoparticles in the concentration of 0.1 g/L at the working zone fundamentally changes the electrical condition in the interelectrode gap [64].

It improves the material removal rate by ~6 times compared to triple copper tape and by ~30 times compared to silver double coating sandwich with Ag nanopowder.

The authors of [66] noticed that the programmed depth faster was achieved with a thicker conductive layer in a hydrocarbon medium. However, the authors reported that they did not understand the processes' chemical nature during the electrical discharge machining of Al_2O_3 and ZrO_2 ceramics, which needs additional research and explanation from the thermo- and electrochemistry point of view.

It is noticed that during electrical discharge machining of Si_3N_4 insulating ceramics, carbon-containing substances of the kerosene under high temperatures are often cracked and stuck to the positive pole in the voltage field [17]. The electrically conductive material adhered to the insulating workpiece's surface during the electrical discharge machining of Si_3N_4 , ZrO_2 in kerosene. It consisted of decomposable carbon-containing substances from the fluid that can be conductive carbides of the ZrC group and semiconductive SiC adhered to the insulating workpiece surface. An electrically conductive carbide layer was formed during continuously generated electrical discharges. Thus, insulating ceramics are transformed into electrically machinable material during electrical discharge machining. However, during the electrical discharge machining of the sintered $\text{Al}_2\text{O}_3 + 20\%$ of ZrO_2 stabilized with 3.9% of Y_2O_3 in kerosene, the conductive layer was not specified [78], obviously due to the known insulating properties of Al_3C_4 . The eroded layer was removed mechanically after electrical discharge machining.

A standard silver varnish with 45% silver content was used to create the conductive layer of approximately 20 μm on the surface of ZrO_2 ceramics [71]. After drying, the layer formation's uniformity was tested by measuring the resistance using a Fluke multimeter. When the first layer was machined, a conducting rebuilt layer was generated on the workpiece, visible as black surface areas. The detailed composition of this layer was not under investigation. Still, it can be proposed that due to the thermal decomposition of the hydrocarbon oil by the electrical discharges and following plasma channel, ZrC was formed.

With an assisting electrode applied by a screen printing when electrical discharge machining of a semi-conductive silicon carbide [79] that did not exhibit electrical conductivity, the process was initially unstable, and it required the adjustment of machining factors such as current and frequency and tool geometry. The authors found that the cause of unstable machining might be the excessive generation of carbonized products. The average thickness of the carbonized layer on the ceramic surface was 24 μm with a standard deviation of 1.6 μm . The adaptation of tool geometry was produced to improve flushing in the working area. The maximum machined depth was 420 μm . The maximum material removal rate was $3.58 \times 10^{-3} \text{ mm}^3/\text{min}$ (~0.215 mm^3/s). Detached microstructures with an aspect ratio of 30 are machined. The present material removal mechanism was indicated as thermally induced spalling. No heat-affected zone was detected. The same group of researchers studied the electrical discharge machining of SiC-based composites [80]. The assisting electrode was generated from the decomposed dielectric oil and deposited on the ceramic surface. It is found that the conductivity of the SiC-based materials does not influence the machinability of ceramics' microtexturing.

The suitable factors to accomplish the electrical discharge machining of insulating ceramics are the following:

- Assisting electrode material—copper tape/foil, silver coating/varnish, carbon tape, Cu + Ag sandwich, Ni + Cr PVD-coating;
- Assisting electrode thickness—from 12 to 300 μm ;
- Type of assisting electrode deposition—adhesive, diffusion;
- Assisting powder material—Ag nanoparticles, graphite, SnO, TiO_2 , ZnO;
- Assisting powder granule size—from nano size to 10–30 μm in diameter;
- Assisting powder concentration for suspension of 0.1–150 g/L;
- Operational current of 0.3–0.4 A;
- Operational voltage of 108 V;

- The frequency of 2, 5, 7, 10, 30 kHz;
- Pulse duration of 0.5–2.5 μs ;
- The discharge gap of 48–60 μm .

4. Discussion

Let us represent the summarized data on machinability via EDM presented in Tables 3 and 4 in the form of graphs to approximate the obtained graphs up to the closest functions and analyze the revealed dependencies.

The dependence of conductive ceramic composites' machinability via electrical discharge machining on electrical conductivity for some conductive ceramic composites based on Table 3 is presented in Figure 8. As can be seen, the dependence has a character of the logarithmic regression with a coefficient of determination of 0.7066:

The higher the electrical conductivity, the higher the machinability.

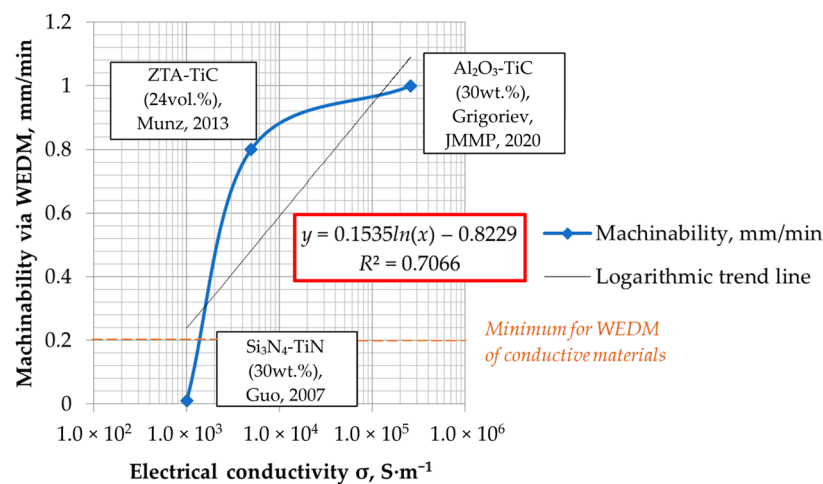


Figure 8. The dependence of conductive ceramic composites' machinability via wire electrical discharge machining on electrical conductivity, where R^2 is a coefficient of determination, Grigoriev, JMMP, 2020 [11], Munz, 2013 [46], Guo, 2007 [50].

Figure 9 presents graphs based on data from Table 4 depending on the specific resistance of the assisting coatings, the band gap, and the concentration of the assisting powder. The data are provided for Al_2O_3 and AlN ceramics. As it is seen in Figure 9a, the material removal rate is in inverse relationship with the specific resistance of the assisting coatings, and it is evident that despite the conviction of many authors that it is the electrical properties of the assisting coating that play a key role in the machinability of insulating ceramics. There should be the influence of other factors previously overlooked by the authors when developing a research plan and selecting an assisting electrode material. Figure 9b demonstrates the exponential relationship between the material removal rate and the band gap of the assisting powder for Al_2O_3 ceramics machined in hydrocarbons and water suspension (as more band gap is, as more dielectric properties exhibit material, up to 3–4 eV for semiconductors and more than 4–5 eV for dielectrics). Thus, the machinability dependence on the assisting powder's electrical properties is proven:

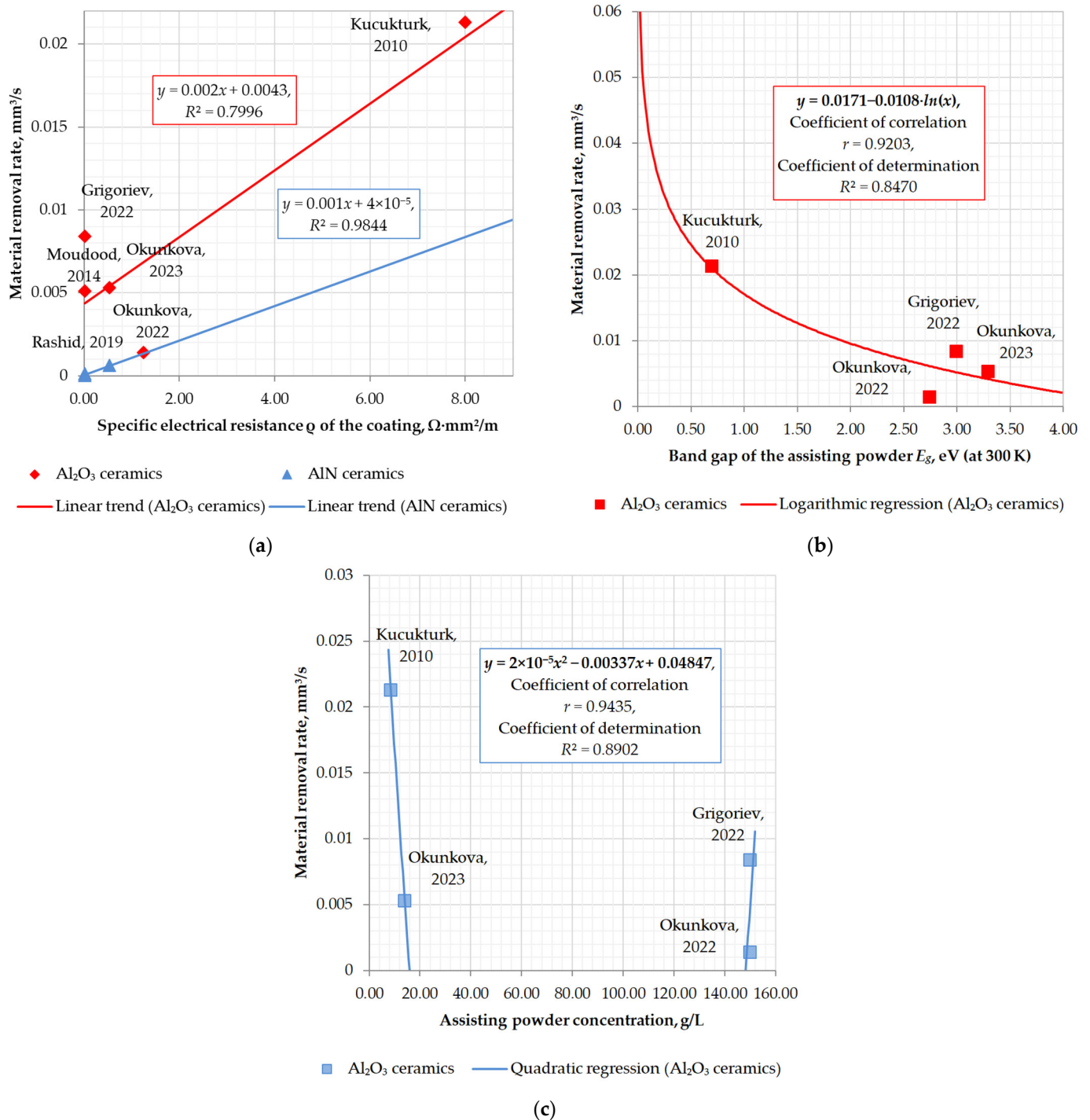


Figure 9. The graphical presentation of Al-containing insulating ceramic machinability via electrical discharge machining: (a) dependence on the specific electrical resistance of the assisting coating; (b) dependence on the band gap of the assisting powder; (c) dependence on the assisting powder concentration, where Moudood, 2014 [63], Rashid, 2019 [64], Grigoriev, 2022 [65], Kucukturk, 2010 [66], Okunkova, 2023 [67], Okunkova, 2022 [68].

The lower the band gap, the higher the machinability.

The graph presents the results of the approximation. That is a logarithmic regression of the following type:

$$y = y_0 \cdot (b - a \cdot \ln(x)), \tag{13}$$

where a and b are empirical coefficients and require additional research. The data presented in Figure 9c are correlated with the data obtained in [65,67], where the assisting powder concentration influence on the material removal rate was researched in the concentration gap of 50–150 g/L and 7–100 g/L, correspondingly. The most pronounced results were achieved at 14 and 150 g/L. The reduction in machinability was observed in the range of the powder concentration from 21 to 100 g/L. The dependence corresponds to the quadratic regression as follows:

$$y = y_0 \cdot (a \cdot x^2 + b \cdot x + c) \quad (14)$$

and can be a part of the logarithmic decrement of attenuation of the following type:

$$y = y_0 \cdot e^{-a \cdot x} \quad (15)$$

that seems more relevant to the mathematical expression of physical phenomena and requires more study.

For further development, it should be noted that TiO₂ and ZnO are semiconductive with a band gap of 3.00–3.26 eV for TiO₂ depending on its form (for anatase is more than for rutile) and ~3.37 eV for ZnO. It can be quite a perspective to consider adding other semiconductors with lower band gap values to improve conductivity conditions in the interelectrode gap. However, most of them as Cd₃As₂, Cd₃P₂, SnTe, VO₂, Zn₃P₂ (the band gap of ~0, 0.5, 0.18, 0.7, 1.5 eV correspondingly [81–85]) are highly poisonous (4 points for health by NFPA 704). This excludes any possibility of their development and uses in the conditions of real production in the future. However, two of them deserve attention for further consideration—copper sulfides (Cu_xS_y) and rare Tin(II) sulfide (α-SnS) with band energies of ~1.2 and 1.0–1.3 eV, correspondingly. They are available on the market in powder form.

Solving the problems of electrical discharge machining application techniques for aluminum-containing ceramics is of fundamental importance for science and applications such as electric power, the space industry, optics, and a promising cutting tool made of cutting ceramics. The development of superhard and highly wear- and heat-resistant materials based on ceramics with

- A low coefficient of linear thermal expansion ($\alpha \times 10^6$ of 7.0–8.0 K⁻¹ for Al₂O₃, 4.0–6.0 K⁻¹ for AlN, 3.0 K⁻¹ for SiAlON at 20–1000 °C);
- Low thermal conductivity at normal temperatures (λ of 22–25 W·(m·K)⁻¹ for Al₂O₃, > 170 W·(m·K)⁻¹ for AlN, 85 W·(m·K)⁻¹ for SiAlON at 20–100 °C); and
- Excellent optical properties (spectral transmission range of 0.17–5.5 μm for Al₂O₃, 0.2–5.0 μm for thin films of AlN [86], 2.5–5.0 for SiAlON [87]) by volumetric shaping will make it possible to create a group of new classes of metal-cutting tools with exceptional exploitation properties.

These tools can be aimed at machining high-entropy alloys, such as nickel- and titanium-based alloys achieving 800–1000 °C in the contact zone in friction pair [70,88], and carry out the sixth technological transition associated with Kondratieff's waves [89,90].

The better results for the electrical discharge machining of insulating ceramics using assisting means can be summarized as follows (Table 5).

Table 5. The summarized results of electrical discharge machining of insulating ceramics.

Insulating Ceramics	Assisting Electrode (Coating) Material/Type of Deposition	Assisting Electrode Thickness, μm	Dielectric Medium	Assisting Powder	Primary Electrode Material and Shape	Adhered Material at the Primary Electrode	Theoretical Chemical Composition of the Assisting Debris [24,39]	Material Removal rate, mm^3/s	Reference
Al_2O_3	Copper tape/adhesive	40	Water-based suspension	TiO_2 particles of $\varnothing 10 \mu\text{m}$ (150 g/L) SnO particles of $\varnothing 10 \mu\text{m}$ (150 g/L)	Brass wire, $\varnothing 250 \mu\text{m}$	Not reported	Cu^{2+} (conductive)	0.0084	[65]
	Ni-Cr coating/diffusion	12			Brass wire, $\varnothing 250 \mu\text{m}$	Not reported	Al_xNi_y (conductive)	0.014	[68]
AlN	Ag nanoparticles sandwiched between two layers of Ag varnish with Cu tape on top/adhesive	Not provided	Hydrocarbon oil, no flushing, no rotation	Ag nanoparticle (0.1 g/L)	Cu-W, $\varnothing 308 \mu\text{m}$	Not reported	Ag^{1+} (conductive)	0.0006 *	[64]
Si_3N_4	Not provided (expected TiN coating/diffusion based on [18]) †	Not provided	Kerosene oil, rotation at 100 min^{-1}	Not provided	Cu, $\varnothing 2000 \mu\text{m}$	SiC (semi-conductive)	SiC (semi-conductive)/TiC (conductive)/TiN (conductive)	-0.51–0.84	[59]
TiO_2	Carbon tape (polymer-based)/adhesive	Not provided	Kerosene, flushing at 1.5 bar pressure	Graphite powder of $\varnothing 30 \mu\text{m}$ (7–10 g/L)	Cu pipe of $\varnothing 3500 \mu\text{m}$ with a hole of $\varnothing 3000 \mu\text{m}$	TiC (conductive)	TiC (conductive)	-0.45	[66]
ZrO_2						ZrC (conductive)	ZrC (conductive)	-0.55	

* calculated for convenience; † the authors did not provide data on the conductive layer but have mentioned using it; based on similar works [18], it can be concluded that TiN coating deposited by PVD was used.

5. Conclusions

The conducted review allowed the recent advances in the electrical discharge machining of insulating ceramics to be summarized and analyzed, and revealed the dependences of the machinability on:

- The electrical properties of the ceramics for conductive ceramic composites (logarithmic regression);
- The specific electrical resistance of the assisting coating (needs additional research), the band gap (logarithmic regression) and the powder concentration of the assisting powder (quadratic regression) for insulating ceramics.

It has been shown that the lower the band gap, the higher the machinability. There are summarized data on electrical discharge machining factors for conductive ceramic composites and insulating ceramics.

The proposed approach of using the semiconductive powder composition with the small band gap can be extended to develop solutions for electrical discharge machining other insulating materials.

The electrical discharge machining of insulating ceramics has vast potential. It requires transitioning from laboratory conditions to real industrial applications to process reinforcing ceramics and other new ceramic-based composites to produce:

- A novel helical cutting tool with exploitation properties that can be of a critical advantage in milling new nickel- and titan-based and superalloys above $800 \text{ }^\circ\text{C}$ close to or even exceeding the properties of the pure sintered oxide and nitride ceramics;
- A new nanocomposite with physical properties that exceed the properties of the known materials in electrical resistivity, hot hardness, resistance to abrasive wear, linear thermal expansion, and thermal conductivity that can be not available to be shaped by traditional milling and turning due to their exceptional properties for aerospace applications.

The existing technological approaches in electrical discharge machining insulating ceramics have no advantages or disadvantages. The technology itself is not suitable for machining insulating materials and, by the existing logic, should not provide any results. However, some researchers put their efforts into exploring the limits of the existing technology of electrical discharge machining without putting any mechanical effort on the surface of the insulating materials using special measures such as providing an electrically conductive layer on the surface of the insulating ceramics. The machining is performed using the thermal effect of the electrical discharges, providing conductive particles and/or debris in the discharge gap to make the discharges denser and changing the electrical conditions in the interelectrode gap. The most outstanding in this context is the fact that many research groups achieve the machinability of the insulating ceramics by electrical

discharge machining that is much less than for the convenient conductive materials but still shows impressive data (up to 0.0051–0.0213 mm³/s).

Author Contributions: Conceptualization, S.N.G.; methodology, M.A.V.; software, A.A.O.; validation, M.A.V.; formal analysis, A.A.O.; investigation, A.A.O.; resources, M.A.V.; data curation, M.A.V.; writing—original draft preparation, A.A.O.; writing—review and editing, M.A.V.; visualization, A.A.O.; supervision, S.N.G.; project administration, S.N.G.; funding acquisition, S.N.G. All authors have read and agreed to the published version of the manuscript.

Funding: This work was supported financially by the Ministry of Science and Higher Education of the Russian Federation (project No. FSFS-2021-0003).

Institutional Review Board Statement: Not applicable.

Informed Consent Statement: Not applicable.

Data Availability Statement: Data are available in a publicly accessible repository.

Acknowledgments: This study was carried out on the equipment of the Center of collective use of MSUT “STANKIN” supported by the Ministry of Higher Education of the Russian Federation (project No. 075-15-2021-695 from 26 July 2021, unique identifier RF 2296.61321 × 0013).

Conflicts of Interest: The authors declare no conflict of interest.

References

1. Grigoriev, S.N.; Nadykto, A.B.; Volosova, M.A.; Zelensky, A.A.; Pivkin, P.M. WEDM as a Replacement for Grinding in Machining Ceramic Al₂O₃-TiC Cutting Inserts. *Metals* **2021**, *11*, 882.
2. Bocharov, G.S.; Eletsii, A.V.; Knizhnik, A.A. Nonlinear resistance of polymer composites with carbon nanotube additives in the percolation state. *Tech. Phys.* **2016**, *61*, 1506–1510. [[CrossRef](#)]
3. Zholnin, A.G.; Tenishev, A.V.; Stolyarov, V.V. Effect of the Thermomechanical Compacting Conditions on the Electrical Conductivity of an Al₂O₃/Graphene Composite Material. *Russ. Metall.* **2019**, *10*, 1009–1014. [[CrossRef](#)]
4. Karpov, A.V.; Konovalikhin, S.V.; Borovinskaya, I.P.; Sachkova, N.V.; Kovalev, D.Y.; Sytshev, A.E. Conductive TiB₂-AlN-BN-Based Composite SHS Ceramics. *Russ. J. Non-Ferr. Met.* **2018**, *59*, 658–663.
5. Melnik, Y.A.; Kozochkin, M.P.; Porvatov, A.N.; Okunkova, A.A. On Adaptive Control for Electrical Discharge Machining Using Vibroacoustic Emission. *Technologies* **2018**, *6*, 96. [[CrossRef](#)]
6. Lukianova, O.A.; Khmara, A.N.; Perevislov, S.N.; Kolesnikov, D.A.; Krasilnikov, V.V. Electrical resistivity of silicon nitride produced by various methods. *Ceram. Int.* **2019**, *45*, 9497–9501.
7. Rumiantseva, Y.Y.; Romanko, L.O.; Chasnyk, D.V.; Turkevich, V.Z.; Bushlya, V.M.; Fesenko, I.P.; Kaidash, O.M.; Chasnyk, V.I.; Rukin, V.P. Electrical Characteristics of Thermobarically Sintered cBN-NbN Composite. *J. Superhard Mater.* **2020**, *42*, 126–128.
8. Vellaikal, M.; Kingon, A.I. Electrical and microstructural characterization of lead titanate thin films deposited by metal-organic chemical vapor deposition onto platinum and magnesium oxide. *Thin Solid Film.* **1996**, *287*, 139–145. [[CrossRef](#)]
9. Kang, T.K.; Kim, S.J. Variations in The Electrical-Resistivity of Y₂O₃-Doped ZrO₂ Ceramics with Microstructural Design. *J. Phys. Condens. Matter* **1994**, *6*, 4343–4350.
10. Jiang, Y.; Wu, L.; Sun, W.Z. Influence of Sintering Additives and TiC on Properties of TiC/Si₃N₄ Ceramics. *Powders Grains* **2013**, *1542*, 125–128.
11. Grigoriev, S.N.; Volosova, M.A.; Okunkova, A.A.; Fedorov, S.V.; Hamdy, K.; Podrabinnik, P.A.; Pivkin, P.M.; Kozochkin, M.P.; Porvatov, A.N. Electrical Discharge Machining of Oxide Nanocomposite: Nanomodification of Surface and Subsurface Layers. *J. Manuf. Mater. Process.* **2020**, *4*, 96.
12. Lengauer, W.; Binder, S.; Aigner, K.; Ettmayer, P.; Guillou, A.; Debuigne, J.; Groboth, G. Solid-State Properties of Group IVB Carbonitrides. *J. Alloys Compd.* **1995**, *217*, 137–147.
13. Shahzad, F.; Iqbal, A.; Kim, H.; Koo, C.M. 2D Transition Metal Carbides (MXenes): Applications as an Electrically Conducting Material. *Adv. Mater.* **2020**, *32*, 2002159.
14. Tantardini, C.; Oganov, A.R. Thermochemical electronegativities of the elements. *Communications* **2021**, *12*, 2087. [[CrossRef](#)] [[PubMed](#)]
15. Selvarajan, L.; Sathiyarayanan, C.; Jeyapaul, R.; Manohar, M. Optimization of EDM process parameters in machining Si₃N₄-TiN conductive ceramic composites to improve form and orientation tolerances. *Meas. J. Int. Meas. Confed.* **2016**, *92*, 114–129.
16. Lazar, I.; Majchrowski, A.; Soszyński, A.; Roleder, K. Phase Transitions and Local Polarity above T_C in a PbZr_{0.87}Ti_{0.13}O₃ Single Crystal. *Crystals* **2020**, *10*, 286.
17. Deng, G.Q.; Guo, Y.F.; Peng, Q.J.; Lu, Z.S.; Bai, J.C. A Novel Discharging Status Distinguish Method on Machining Si₃N₄ by HS-WEDM. In Proceedings of the 16th International Symposium on Electromachining, ISEM 2010, Shanghai, China, 19–23 April 2010; pp. 275–278.

18. Fukuzawa, Y.; Tani, T.; Mohri, N. Machining characteristics of insulated Si₃N₄ ceramics by electrical discharge method—Use of powder-mixed machining fluid. *J. Ceram. Soc. Jpn.* **2000**, *108*, 184–190. [[CrossRef](#)]
19. Volosova, M.; Okunkova, A.; Peretyagin, P.; Melnik, Y.A.; Kapustina, N. On Electrical Discharge Machining of Non-Conductive Ceramics: A Review. *Technologies* **2019**, *7*, 55.
20. Tian, X.; Zhao, J.; Wang, Y.; Gong, F.; Qin, W.; Pan, H. Fabrication and mechanical properties of Si₃N₄/(W, Ti)C/Co graded nano-composite ceramic tool materials. *Ceram. Int.* **2015**, *41*, 3381–3389.
21. Habib, S.S. Study of the parameters in electrical discharge machining through response surface methodology approach. *Appl. Math. Model.* **2009**, *33*, 4397–4407.
22. Cheng, M.; Liu, H.; Zhao, B.; Huang, C.; Yao, P.; Wang, B. Mechanical properties of two types of Al₂O₃/TiC ceramic cutting tool material at room and elevated temperatures. *Ceram. Int.* **2017**, *43*, 13869–13874. [[CrossRef](#)]
23. Wang, D.; Xue, C.; Cao, Y.; Zhao, J. Fabrication and cutting performance of an Al₂O₃/TiC/TiN ceramic cutting tool in turning of an ultra-high-strength steel. *Int. J. Adv. Manuf. Technol.* **2017**, *91*, 1967–1976. [[CrossRef](#)]
24. Volosova, M.A.; Okunkova, A.A.; Fedorov, S.V.; Hamdy, K.; Mikhailova, M.A. Electrical Discharge Machining Non-Conductive Ceramics: Combination of Materials. *Technologies* **2020**, *8*, 32.
25. Gevorkyan, E.; Rucki, M.; Panchenko, S.; Sofronov, D.; Chaiko, L.; Mazur, T. Effect of SiC Addition to Al₂O₃ Ceramics Used in Cutting Tools. *Materials* **2020**, *13*, 5195. [[CrossRef](#)] [[PubMed](#)]
26. Grigoriev, S.N.; Volosova, M.A.; Peretyagin, P.Y.; Seleznev, A.E.; Okunkova, A.A.; Smirnov, A. The Effect of TiC Additive on Mechanical and Electrical Properties of Al₂O₃ Ceramic. *Appl. Sci.* **2018**, *8*, 2385. [[CrossRef](#)]
27. Sevidova, E.K.; Pupan, L.I.; Tsyuryupa, V.N. Influence of Coatings on the Surface Strength of Rapid Prototyping Products. *Surf. Eng. Appl. Electrochem.* **2008**, *44*, 367–369. [[CrossRef](#)]
28. Cui, H.; Chen, Z.; Xiao, G.; Ji, L.; Yi, M.; Zhang, J.; Zhou, T.; Xu, C. Mechanical Properties and Microstructures of Al₂O₃/TiC/TiB₂ Ceramic Tool Material. *Crystals* **2021**, *11*, 637. [[CrossRef](#)]
29. Wahi, R.P.; Ilschner, B. Fracture-Behavior of Composites Based on Al₂O₃-TiC. *J. Mater. Sci.* **1980**, *15*, 875–885. [[CrossRef](#)]
30. Watanabe, M.; Fukuura, I. Strength Of Al₂O₃ and Al₂O₃-TiC Ceramics in Relation to Their Fracture Sources. *Am. Ceram. Soc. Bull.* **1981**, *60*, 394.
31. Movchan, B.A.; Grechanyuk, N.I. Microhardness And Microbrittleness of Condensates of the TiC- Al₂O₃ System. *Inorg. Mater.* **1981**, *17*, 972–973.
32. Verdi, C.; Karsai, F.; Liu, P.T.; Jinnouchi, R.; Kresse, G. Thermal transport and phase transitions of zirconia by on-the-fly machine-learned interatomic potentials. *NPJ Comput. Mater.* **2021**, *7*, 156. [[CrossRef](#)]
33. Borik, M.A.; Volkova, T.V.; Kulebyakin, A.V.; Kuritsyna, I.E.; Lomonova, E.E.; Myzina, V.A.; Milovich, F.O.; Ryabochkina, P.A.; Tabachkova, N.Y.; Zentsova, A.I.; et al. Thermal Conductivity of Cubic ZrO₂ Single Crystals Stabilized with Yttrium Oxide. *Phys. Solid State* **2020**, *62*, 235–239. [[CrossRef](#)]
34. Liu, D.M.; Tuan, W.H. Microstructure and its influence on thermal and electrical conductivity of ZrO₂-Ag composites. *Mater. Chem. Phys.* **1997**, *48*, 258–262. [[CrossRef](#)]
35. Melk, L.; Antti, M.L.; Anglada, M. Material removal mechanisms by EDM of Zirconia reinforced MWCNT nanocomposites. *Ceram. Int.* **2016**, *42*, 5792–5801. [[CrossRef](#)]
36. Tu, R.; Xiao, B.; Zhang, S.; Deng, Z.; Li, Q.Z.; Yang, M.J.; Goto, T.; Zhang, L.M.; Ohmori, H. Mechanical, electrical and thermal properties of ZrC-ZrB₂-SiC ternary eutectic composites prepared by arc melting. *J. Eur. Ceram. Soc.* **2018**, *38*, 3759–3766. [[CrossRef](#)]
37. Dewi, A.K.; Yamaguchi, S.; Onitzuka, T.; Uno, M. Thermal conductivity calculation of ZrC-ZrO₂ pellet from powder metallurgy as the surrogate of UCO kernel fuel. *J. Nucl. Mater.* **2020**, *539*, 152343. [[CrossRef](#)]
38. Uporov, S.; Bykov, V.; Estemirova, S. Electrical and thermal conductivities of rapidly crystallized Cu-Zr alloys: The effect of anharmonicity. *Phys. B-Condens. Matter* **2016**, *499*, 97–106. [[CrossRef](#)]
39. Gao, L.; Guan, R.; Zhang, S.; Zhi, H.; Jin, C.; Jin, L.; Wei, Y.; Wang, J. As-Sintered Manganese-Stabilized Zirconia Ceramics with Excellent Electrical Conductivity. *Crystals* **2022**, *12*, 620. [[CrossRef](#)]
40. Boskovic, S.; Sigulinski, F.; Zivkovic, L. Liquid-phase sintering and properties of Si₃N₄-TiN composites. *J. Mater. Synth. Process.* **1999**, *7*, 119–126. [[CrossRef](#)]
41. Zhang, S.H.; Kang, Z.Q.; Lu, Q. Room-temperature electrical conductivity property of Si₃N₄/TiN composite ceramics. *Adv. Mater. Res.* **2011**, *150*, 257–261.
42. Xu, J.H.; Gu, M.Y.; Li, G.Y.; Jin, Y.P. Microstructures and properties of Si₃N₄/TiN ceramic nano-multilayer films. *Trans. Nonferrous Met. Soc. China* **1999**, *9*, 764–767.
43. L'vov, B.V. *Thermal Decomposition of Solids and Melts New Thermochemical Approach to the Mechanism, Kinetics and Methodology*; Springer Science & Business Media: Berlin/Heidelberg, Germany, 2007; ISBN 978-1-4020-5672-7.
44. Grigoriev, S.; Pristinskiy, Y.; Volosova, M.; Fedorov, S.; Okunkova, A.; Peretyagin, P.; Smirnov, A. Wire Electrical Discharge Machining, Mechanical and Tribological Performance of TiN Reinforced Multiscale SiAlON Ceramic Composites Fabricated by Spark Plasma Sintering. *Appl. Sci.* **2021**, *11*, 657. [[CrossRef](#)]
45. Schubert, A.; Zeidler, H.; Kühn, R.; Hackert-Oschätzchen, M.; Flemmig, S.; Treffkorn, N. Investigation of Ablation Behaviour in Micro-EDM of Nonconductive Ceramic Composites ATZ and Si₃N₄-TiN. *Procedia CIRP* **2016**, *42*, 727–732. [[CrossRef](#)]
46. Munz, M.; Risto, M.; Haas, R.; Landfried, R.; Kern, F.; Gadow, R. Machinability of ZTA-TiC ceramics by electrical discharge drilling. *Procedia CIRP* **2013**, *6*, 77–82. [[CrossRef](#)]

47. Quarto, M.; Bissacco, G.; D'Urso, G. Study on ZrB₂-Based Ceramics Reinforced with SiC Fibers or Whiskers Machined by Micro-Electrical Discharge Machining. *Micromachines* **2020**, *11*, 959. [[CrossRef](#)]
48. Grigoriev, S.N.; Volosova, M.A.; Okunkova, A.A.; Fedorov, S.V.; Hamdy, K.; Podrabinnik, P.A.; Pivkin, P.M.; Kozochkin, M.P.; Porvatov, A.N. Wire Tool Electrode Behavior and Wear under Discharge Pulses. *Technologies* **2020**, *8*, 49. [[CrossRef](#)]
49. Gavrin, V.N.; Kozlova, Y.P.; Veretenkin, E.P.; Logachev, A.V.; Logacheva, A.I.; Lednev, I.S.; Okunkova, A.A. Reactor target from metal chromium for "pure" high-intensive artificial neutrino source. *Phys. Part. Nucl. Lett.* **2016**, *13*, 267–273. [[CrossRef](#)]
50. Guo, Z.; Blugan, G.; Kirchner, R.L.; Reece, M.; Graule, T.; Kuebler, J. Microstructure and electrical properties of Si₃N₄-TiN composites sintered by hot pressing and spark plasma sintering. *Ceram. Int.* **2007**, *33*, 1223–1229. [[CrossRef](#)]
51. Nikitin, P.; Zhukov, I.; Matveev, A.; Sokolov, S.; Sachkov, V.; Vorozhtsov, A. Phase Composition, Structure and Properties of the Spark Plasma Sintered Ceramics Obtained from the Al₁₂Mg₁₇-B-Si Powder Mixtures. *Nanomaterials* **2022**, *12*, 1895. [[CrossRef](#)]
52. Niamat, M.; Sarfraz, S.; Shehab, E.; Ismail, S.O.; Khalid, Q.S. Experimental characterization of electrical discharge machining of aluminum 6061 T6 alloy using different dielectrics. *Arab. J. Sci. Eng.* **2019**, *44*, 8043–8052. [[CrossRef](#)]
53. Ablyaz, T.R.; Bains, P.S.; Sidhu, S.S.; Muratov, K.R.; Shlykov, E.S. Impact of Magnetic Field Environment on the EDM Performance of Al-SiC Metal Matrix Composite. *Micromachines* **2021**, *12*, 469. [[CrossRef](#)]
54. Hanaoka, D.; Ito, R.; Fukuzawa, Y. Electrical Discharge Machined Surface of the Insulating ZrO₂ Ceramics. *J. Adv. Mech. Des. Syst. Manuf.* **2011**, *5*, 372–384. [[CrossRef](#)]
55. Kansal, H.K.; Singh, S.; Kumar, P. Technology and research developments in powder mixed electric discharge machining (PMEDM). *J. Mater. Process. Technol.* **2007**, *184*, 32–41. [[CrossRef](#)]
56. Lin, Y.J.; Lin, Y.C.; Wang, A.C.; Wang, D.A.; Chow, H.M. Machining characteristics of EDM for non-conductive ceramics using adherent copper foils. *Adv. Mater. Res.* **2011**, *154*, 794–805.
57. Zhang, H.; Liu, Y.; Chen, J.; Shen, R.; Cai, B.; Wang, D. Experimental research on pulse generator for EDM of non-conductive ceramics. *Key Eng. Mater.* **2009**, *407*, 649–653.
58. Ojha, N.; Zeller, F.; Mueller, C.; Reinecke, H. Analyzing the electrical pulses occurring during EDM of non-conductive Si₃N₄ ceramics. *Key Eng. Mater.* **2015**, *651*, 659–664.
59. Gotoh, H.; Tani, T.; Mohri, N. EDM of Insulating Ceramics by Electrical Conductive Surface Layer Control. *Procedia CIRP* **2016**, *42*, 201–205. [[CrossRef](#)]
60. Ramezani, Z.; Saeedi, I.; Hashemi, P. Dendrimer grafted nanoporous silica fibers for headspace solid phase microextraction coupled to gas chromatography determination of solvent residues in edible oil. *Anal. Methods* **2018**, *10*, 1379–1384. [[CrossRef](#)]
61. Park, D.W.; Jang, S.; Nam, B.J.; Ham, C.; Lim, S.T. Chemical Cleaning of Iron Stains on Ceramics. *J. Conserv. Sci.* **2011**, *27*, 345–356.
62. Liu, Y.H.; Li, X.P.; Ji, R.J.; Yu, L.L.; Zhang, H.F.; Li, Q.Y. Effect of technological parameter on the process performance for electric discharge milling of insulating Al₂O₃ ceramic. *J. Mater. Process. Technol.* **2008**, *208*, 245–250. [[CrossRef](#)]
63. Moudood, M.A.; Sabur, A.; Mohammad, Y.A.; Jaafar, I.H. Effect of Peak Current on Material Removal Rate for Electrical Discharge Machining of Non-conductive Al₂O₃ Ceramic, Materials, Industrial, And Manufacturing Engineering Research Advances 1.1. *Adv. Mater. Res.* **2014**, *845*, 730–734.
64. Rashid, A.; Bilal, A.; Liu, C.; Jahan, M.P.; Talamona, D.; Perveen, A. Effect of Conductive Coatings on Micro-Electro-Discharge Machinability of Aluminum Nitride Ceramic Using On-Machine-Fabricated Microelectrodes. *Materials* **2019**, *12*, 3316. [[CrossRef](#)]
65. Grigoriev, S.N.; Okunkova, A.A.; Volosova, M.A.; Hamdy, K.; Metel, A.S. Electrical Discharge Machining of Al₂O₃ Using Copper Tape and TiO₂ Powder-Mixed Water Medium. *Technologies* **2022**, *10*, 116. [[CrossRef](#)]
66. Kucukurtk, G.; Cogun, C. A New Method for Machining of Electrically Nonconductive Workpieces using Electric Discharge Machining Technique. *Mach. Sci. Technol.* **2010**, *14*, 189–207. [[CrossRef](#)]
67. Okunkova, A.A.; Volosova, M.A.; Hamdy, K.; Gkhashim, K.I. Electrical Discharge Machining of Alumina Using Cu-Ag and Cu Mono- and Multi-Layer Coatings and ZnO Powder-Mixed Water Medium. *Technologies* **2023**, *11*, 6. [[CrossRef](#)]
68. Okunkova, A.A.; Volosova, M.A.; Kropotkina, E.Y.; Hamdy, K.; Grigoriev, S.N. Electrical Discharge Machining of Alumina Using Ni-Cr Coating and SnO Powder-Mixed Dielectric Medium. *Metals* **2022**, *12*, 1749. [[CrossRef](#)]
69. Sabur, A.; Ali, M.Y.; Maleque, M.A.; Khan, A.A. Investigation of material removal characteristics in EDM of nonconductive ZrO₂ ceramic. *Procedia Eng.* **2013**, *56*, 696–701. [[CrossRef](#)]
70. Volosova, M.A.; Okunkova, A.A.; Hamdy, K.; Malakhinsky, A.P.; Gkhashim, K.I. Simulation of Mechanical and Thermal Loads and Microtexturing of Ceramic Cutting Inserts in Turning a Nickel-Based Alloy. *Metals* **2023**, *13*, 1241. [[CrossRef](#)]
71. Schubert, A.; Zeidler, H.; Hahn, M.; Hackert-Oschätzchen, M.; Schneider, J. Micro-EDM milling of electrically nonconducting zirconia ceramics. *Procedia CIRP* **2013**, *6*, 297–302. [[CrossRef](#)]
72. Guo, Y.; Hou, P.; Shao, D.; Li, Z.; Wang, L.; Tang, L. High-Speed Wire Electrical Discharge Machining of Insulating Zirconia with a Novel Assisting Electrode. *Mater. Manuf. Process.* **2014**, *29*, 526–531. [[CrossRef](#)]
73. Sivkov, A.; Shanenkova, Y.; Vympina, Y.; Nikitin, D.; Shanenkov, I. Deposition of copper coatings on internal aluminum contact surfaces by high-energy plasma spraying. *Surf. Coat. Technol.* **2022**, *440*, 128484. [[CrossRef](#)]
74. Kiani, Z.; Abdi, Y.; Arzi, E. Low Temperature Formation of Silver and Silver-Copper Alloy Nano-Particles Using Plasma Enhanced Hydrogenation and Their Optical Properties. *World J. Nano Sci. Eng.* **2012**, *2*, 142–147. [[CrossRef](#)]
75. Asnis, N.A.; Vasilenko, O.A.; Gasparyan, M.D.; Speshilov, I.O.; Vagramyan, T.A.; Aleshina, V.K. Silvering of High-Porosity Cellular Ceramic Materials. *Russ. J. Appl. Chem.* **2020**, *93*, 1518–1524. [[CrossRef](#)]

76. Wang, H.; Zhang, J.; Yi, M.; Xiao, G.; Chen, Z.; Sheng, C.; Zhang, P.; Xu, C. Simulation study on influence of coating thickness on cutting performance of coated ceramic cutting tools. *J. Phys. Conf. Ser.* **2020**, *1549*, 032140. [[CrossRef](#)]
77. Turchanin, A.A.; Tomilin, I.A.; Inoue, A.S.; Zubkov, A.A. Experimental determination of the formation enthalpies of zirconium-nickel-aluminium amorphous alloys. *Mater. Sci. Eng. A Struct. Mater. Prop. Microstruct. Process.* **1997**, *226*, 487–490. [[CrossRef](#)]
78. Fukuzawa, Y.; Mohri, N.; Gotoh, H.; Tani, T. Three-dimensional machining of insulating ceramics materials with electrical discharge machining. *Trans. Nonferrous Met. Soc. China* **2009**, *19*, s150–s156. [[CrossRef](#)]
79. Zeller, F.; Hösel, T.; Müller, C.; Reinecke, H. Microstructuring of non-conductive silicon carbide by electrical discharge machining. *Microsyst. Technol.* **2014**, *20*, 1875–1880. [[CrossRef](#)]
80. Zeller, F.; Ojha, N.; Müller, C.; Reinecke, H. Electrical Discharge Milling of Silicon Carbide with Different Electrical Conductivity. *KEM* **2014**, *611*, 677–684.
81. Yakovlev, V.A.; Muratov, A.V.; Kucherenko, I.V.; Vinogradov, V.S.; Novikova, N.N.; Karczewski, G.; Schreyeck, S. Structural phase transition and manifestation of eddy currents in IR reflection spectra of PbSnTe semiconductor films. *Quantum Electron.* **2020**, *50*, 263–266. [[CrossRef](#)]
82. Shvetsov, O.O.; Esin, V.D.; Timonina, A.V.; Kolesnikov, N.N.; Deviatov, E.V. Surface superconductivity in a three-dimensional Cd₃As₂ semimetal at the interface with a gold contact. *Phys. Rev. B* **2019**, *99*, 125305. [[CrossRef](#)]
83. Il'inskii, A.V.; Kastro, R.A.; Nikulin, E.I.; Shadrin, E.B. Dielectric Spectroscopy of Strongly Correlated Electronic States of Vanadium Dioxide. *Tech. Phys.* **2018**, *63*, 851–856. [[CrossRef](#)]
84. Gorina, Y.I.; Golubkov, M.V.; Osina, T.Y.; Rodin, V.V.; Sentyurina, N.N.; Chernook, S.G.; Stepanov, V.A. Two-band superconductivity of Sn_{1-x}In_xTe crystals with T_c = 3.6 – 3.8 K. *Phys. Solid State* **2017**, *59*, 1918–1925. [[CrossRef](#)]
85. Polygalov, Y.I.; Poplavnoi, A.S.; Tupitsyn, V.E. Band structure and optical properties of zinc and cadmium diphosphide near the absorption edge. *Semiconductors* **1996**, *30*, 511–513.
86. Drusedau, T.P.; Blasing, J. Optical and structural properties of highly c-axis oriented aluminum nitride prepared by sputter-deposition in pure nitrogen. *Thin Solid Film.* **2000**, *377*, 27–31. [[CrossRef](#)]
87. Liu, Q.; He, W.; Zhong, H.; Zhang, K.; Gui, L. Transmittance improvement of Dy-alpha-SiAlON in infrared range by post hot-isostatic-pressing. *J. Eur. Ceram. Soc.* **2012**, *32*, 1377–1381. [[CrossRef](#)]
88. Migranov, M.S.; Shehtman, S.R.; Sukhova, N.A.; Mitrofanov, A.P.; Gusev, A.S.; Migranov, A.M.; Repin, D.S. Study of Tribotechnical Properties of Multilayer Nanostructured Coatings and Contact Processes during Milling of Titanium Alloys. *Coatings* **2023**, *13*, 171. [[CrossRef](#)]
89. Hamil, R. Is The Wave Of the Future A Kondratieff. *Futurist* **1979**, *13*, 381.
90. Korotayev, A.V.; Tsirel, S.V. A spectral analysis of world GDP dynamics: Kondratiev waves, Kuznets swings, Juglar and Kitchin cycles in global economic development, and the 2008–2009 economic crisis. *Struct. Dyn.* **2010**, *4*, 3–57. [[CrossRef](#)]

Disclaimer/Publisher's Note: The statements, opinions and data contained in all publications are solely those of the individual author(s) and contributor(s) and not of MDPI and/or the editor(s). MDPI and/or the editor(s) disclaim responsibility for any injury to people or property resulting from any ideas, methods, instructions or products referred to in the content.